# Barrier discharges in cellular polypropylene ferroelectrets: How do they influence the electromechanical properties?

Xunlin Qiu,[a] Axel Mellinger, Michael Wegener,[b] Werner Wirges, and Reimund Gerhard
*Applied Condensed-Matter Physics, University of Potsdam, Am Neuen Palais 10, 14469 Potsdam, Germany*

(Received 18 December 2006; accepted 25 March 2007; published online 29 May 2007)

Ferroelectrets (i.e., charged cellular polymers) are rendered piezoelectric by means of barrier discharges inside the air-filled voids. The light emission from barrier discharges in cellular polypropylene ferroelectrets was quantitatively studied. Light emission typically occurs above a threshold voltage of 3 kV and then significantly increases with the applied voltage. Time-resolved images reveal discharge processes in individual voids. In addition, a second "back discharge" emission is observed when the voltage is reduced to zero. The buildup of the "effective polarization" in cellular PP ferroelectrets was studied by an acoustic method and dielectric resonance spectroscopy. A polarization-voltage ($P$-$V$) hysteresis loop was obtained by analyzing the data with an existing model for the piezoelectric $d_{33}$ coefficient of ferroelectrets, from which a threshold charging voltage of 3 kV and the back barrier discharges were confirmed and a zero-field "effective polarization" of 0.5 $mC/m^2$ was determined. However, charge densities of up to 2 $mC/m^2$ were measured under an applied bias voltage, leading to the conclusion that the observed back discharges destroy a significant fraction of the effective charge density. © *2007 American Institute of Physics*. [DOI: 10.1063/1.2735410]

## I. INTRODUCTION

In recent years, a number of cellular and voided polymers were discovered to exhibit a strong quasi-piezoelectric response.[1–3] The piezoelectricity is the result of charges deposited on the internal surfaces of the voids with a typical lateral size of tens of $\mu$m, thus forming electrical dipoles. These materials are now more and more often called "ferroelectrets," because their polarization behavior and other related properties are macroscopically similar to those of typical ferroelectrics, while microscopic charge trapping is the same as in other space-charge electrets.[4]

Ferroelectrets are of considerable interest because they not only broaden the concepts of functional dielectrics, but also show an attractive potential for a variety of applications. The piezoelectricity of ferroelectrets has been theoretically analyzed by means of a model based on charged plane-parallel solid and gaseous layers,[5–8] including finite-element calculations.[9] Work is in progress to develop ferroelectrets based on new polymers with a higher thermal stability.[10–12] Meanwhile, several examples of applications have been reported.[13,14] Much work has recently been done on optimizing the electromechanical properties of ferroelectrets by means of controlled inflation[15–17] and charging in special gas environments.[18,19] It was found that Young's modulus $Y$ has a local minimum upon increasing inflation of the voids, corresponding to a maximum of the piezoelectric $d_{33}$ coefficient. This verifies the proportional relation between $d_{33}$ and $1/Y$ predicted by the model. However, little work has been conducted on the charging process of ferroelectrets, which is the topic of this paper.

Electrical charges are deposited in the voids by means of internal Paschen breakdown that is initiated when the charging voltage becomes higher than a threshold value. In the high external electric field, charges are separated and trapped at the top and bottom surfaces of the voids, resulting in macroscopic dipoles. This charging process in ferroelectrets represents a dielectric barrier discharge (DBD, also referred to as barrier discharge).[20,21] In DBDs, the discharge gap is insulated from the electrodes by dielectric layers. Local breakdown in the gap is initiated by applying an electric field larger than the breakdown field, and charges are transferred through the gap and trapped at the dielectric surfaces. The breakdown extinguishes when the local electrical field, determined by the sum of the electrical field of the accumulated charges and the applied field, becomes lower than the breakdown field. DBDs are widely used for ozone generation, for surface treatment, for pollution control, for excimer lamps[22] and for plasma display panels,[23] and have attracted extensive research.[24] It should be pointed out that DBDs in ferroelectrets are different from the commonly studied ones (these studies are usually dedicated to discharge phenomena in a single dielectric-barrier gap) because of the numerous voids in cellular ferroelectrets with their often rather wide size distribution.

The barrier discharge is accompanied by light emission that can be photographed with a digital camera.[25] Recently, a quantitative analysis of the relation between light emission and piezoelectric activity of layered fluoropolymer ferroelectrets (FEP-ePTFE-FEP sandwiches) was reported.[26] The

[a]Electronic mail: xunlin@canopus.physik.uni-potsdam.de
[b]Present address: Functional Polymer Systems, Fraunhofer Institute for Applied Polymer Research, Geiselbergstrasse 69, 14476 Potsdam-Golm, Germany.

 

ePTFE film in such sandwiches has open pores with a size of 1 $\mu$m. In this paper, we focus on the charging behavior of cellular PP ferroelectrets under the application of suitable voltage waveforms. The closed voids inside cellular PP ferroelectret have a lateral dimension of tens of $\mu$m and a height of several $\mu$m. The light emission from the barrier discharges was quantitatively measured and compared with the buildup of the effective charge density as determined with an acoustic method and dielectric resonance spectroscopy.

## II. SAMPLE PREPARATION

Samples were prepared from a commercial cellular PP film with the trade name PQ50 (Nan Ya Plastics Corporation, Taiwan, China). It is produced by stretching filler-loaded PP under suitable conditions.[27] The initial thickness and density are 50 $\mu$m and 550 kg/m$^3$, respectively. In order to optimize their electromechanical properties, the samples were inflated by gas diffusion expansion in nitrogen and subsequent heat treatment. The samples were then metallized on both sides with semi-transparent gold electrodes having a diameter of 16 mm and a thickness of 20 nm. For optical detection, the edges of the electrodes were covered with silicone rubber to suppress light emission due to corona discharges at the periphery of the electrode layers.

## III. EXPERIMENTS

### A. Charging

The charging voltage was applied directly to the two-side metallized samples by means of a high voltage amplifier (Trek, Model 610) controlled by a function generator (HP 33120a). In addition to amplifying the signal from the function generator, the amplifier is capable of adding a positive or negative dc bias voltage to the ac wave form.

### B. Light emission during charging

The optical emission in the near UV and visible spectral range was studied in a light-tight chamber. The voltage applied to the sample was ramped up at a constant rate, then kept at its maximum value for a certain period of time and finally ramped down at the same rate. The light emission was synchronously measured by a photomultiplier tube (PMT, R7205–01, Hamamatsu) from one side of the sample and by a PC-controlled electron-multiplying charge-coupled device camera (EMCCD, DV887ECS-BV, Andor Technology) from the other side. In order to block any light originating from a corona discharge at the electrode edge, the side of the sample facing the PMT was covered by a mask with a circular hole 8.5 mm in diameter. The PMT signal was captured by a digital storage oscilloscope (Agilent 54833A). The timing of the exposures of the EMCCD camera with respect to the applied voltage ramp was controlled with a delay generator (BNC Model 565, Berkeley Nucleonics).

### C. Acoustic measurements

The measurements were performed in an anechoic chamber. The voltage applied to the sample electrodes consisted of a sinusoidal voltage with a frequency of 1 kHz and an amplitude of 100 V, superimposed on a dc bias voltage. The output sound signal, which is proportional to the amplitude of the vibration of the surface and hence to the actuator sensitivity of the sample, was measured with a microphone (Type 4191, Brüel & Kjaer), connected to a conditioning amplifier (Nexus, Brüel & Kjaer). Both the effective amplitude of the sound signal and its phase shift compared to the applied sinusoidal voltage were recorded with a lock-in amplifier (Model 7280, Ametek Inc.). The recorded sound amplitude is proportional to the inverse piezoelectric $d_{33}$ coefficient of the ferroelectret film. The $d_{33}$ values measured in this way were calibrated by means of dielectric resonance spectroscopy (cf. Sec. III D).

### D. Dielectric resonance spectroscopy

In order to obtain absolute $d_{33}$ values, dielectric resonance spectra were recorded *in situ* using a Novocontrol ALPHA high-resolution dielectric analyzer. The sample was connected to the sample holder via thin silver wires. The dielectric resonance spectrum of a piezoelectric film near the thickness-extension (TE) mode antiresonance frequency is given by[28–30]

$$C(\omega) = \frac{\varepsilon_r \varepsilon_0 A}{h} \frac{1}{1 - k_t^2 \frac{\tan(\omega/4f_p)}{(\omega/4f_p)}} - - iC_{\text{loss}}, \tag{1}$$

where $\varepsilon_r$ is the relative permittivity of the sample, $A$ and $h$ are the electroded sample area and thickness, respectively, $k_t$ is the complex electromechanical coupling factor, and $f_p$ is the complex antiresonance frequency of the TE mode. For a free-standing film, $f_p$ is related to the complex elastic stiffness $c_{33}$ and the sample density $\rho$ by

$$f_p = \frac{1}{2h}\sqrt{\frac{c_{33}}{\rho}}. \tag{2}$$

When one side of the piezoelectric film is glued to a glass substrate, the factor 2 in the denominator must be replaced by 4. The coupling factor $k_t$ is given by

$$k_t^2 = d_{33}^2 c_{33}/(\varepsilon_r \varepsilon_0). \tag{3}$$

From the frequency-dependent real or imaginary part of the capacitance $C(\omega)$, the free parameters $f_p$, $k_t$, $c_{33}$, and $d_{33}$ are determined according to Eqs. (1)–(3) with a least-squares fit.

## IV. RESULTS AND DISCUSSION

### A. Light emission from barrier discharges

The light emission $L(t)$ under different charging voltages is shown in Fig. 1. The ramp-up and ramp-down rate of the charging voltage is kept constant (1 kV/s). Significant light emission starts when the applied voltage exceeds approximately 3 kV. As expected, the light intensity initially rises with the charging voltage because barrier discharges are initiated in an increasing number of voids. In the discharge, positive and negative charges become separated and trapped at the internal surfaces (point A in Fig. 2), thus shielding the void from the external field and extinguishing the discharge.

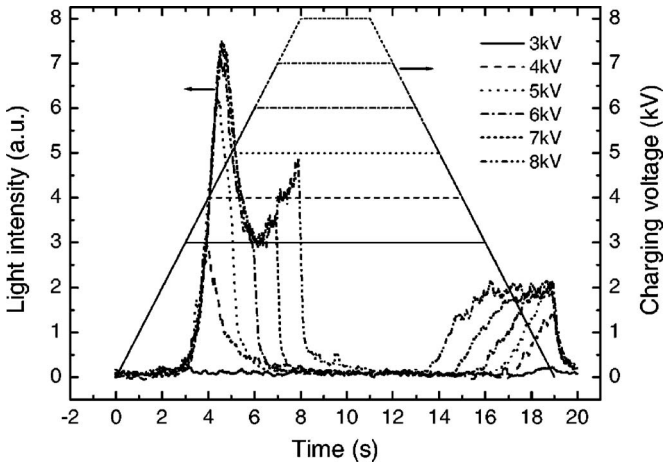


FIG. 1. PMT signal as a function of time under different charging voltages. The voltage ramp rate is ±1 kV/s. For each voltage cycle, a fresh, uncharged sample was used.

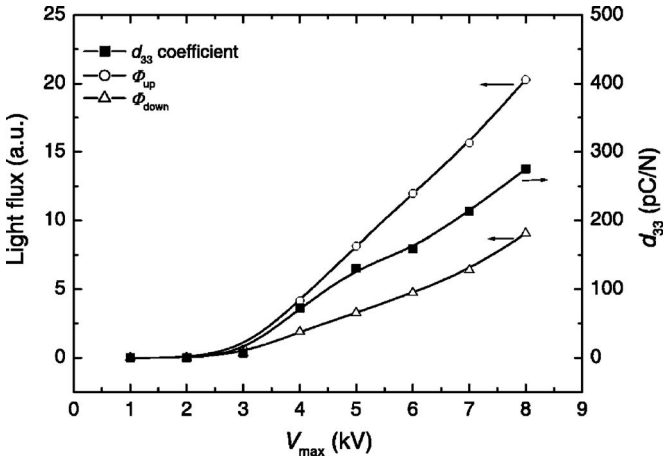


FIG. 3. Light flux during ramping up and during ramping down the charging voltage (experimental data shown in Fig. 1) as a function of the maximum charging voltage. Also shown is the piezoelectric $d_{33}$ coefficient determined from the dielectric resonance spectrum of each sample.

Above 4.5 kV, a significant fraction of the available voids has already experienced Paschen breakdown, resulting in a decrease in the light intensity. When the voltage exceeds approximately 6 kV, however, the emission starts to increase again. This can be understood if voids having experienced a barrier discharge at lower voltages break down again (point B in Fig. 2). Upon reaching the maximum voltage $V_{max}$, the emission decreases sharply to near-zero levels, but starts again during the ramp-down phase when the voltage has dropped to ~3 kV below $V_{max}$. This emission is attributed to a back discharge (inverse barrier discharge). The charges trapped on the top and bottom surfaces of the voids induce an electric field opposite to that of the applied voltage. When the external voltage is reduced, this field may overcompensate the external field and eventually trigger a back discharge (Fig. 2, point C). It should be noted that the back discharge, also called memory behavior, is well known in conventional DBDs.[21] The extent to which this back discharge affects the electromechanical properties of the ferroelectret material will be discussed in the following sections.

The total light flux Φ can be obtained by integrating the light intensity $L(t)$ over time. The light flux during the previously discussed "ramp-up–hold–ramp-down" experiment is shown in Fig. 3 as a function of the maximum charging voltage $V_{max}$. The ramp-up flux

$$\Phi_{up} = \int_0^{t_1} L(t)dt \tag{4}$$

(where $t_1$ is defined in Fig. 2) starts at a threshold voltage of approximately 3 kV and monotonically increases with the charging voltage. It is thus strongly correlated with the piezoelectric $d_{33}$ coefficient, which was calculated from the dielectric resonance spectrum measured immediately after each voltage ramp. Both $\Phi_{up}$ and $d_{33}$ exhibit the same threshold behavior. The back-discharge flux

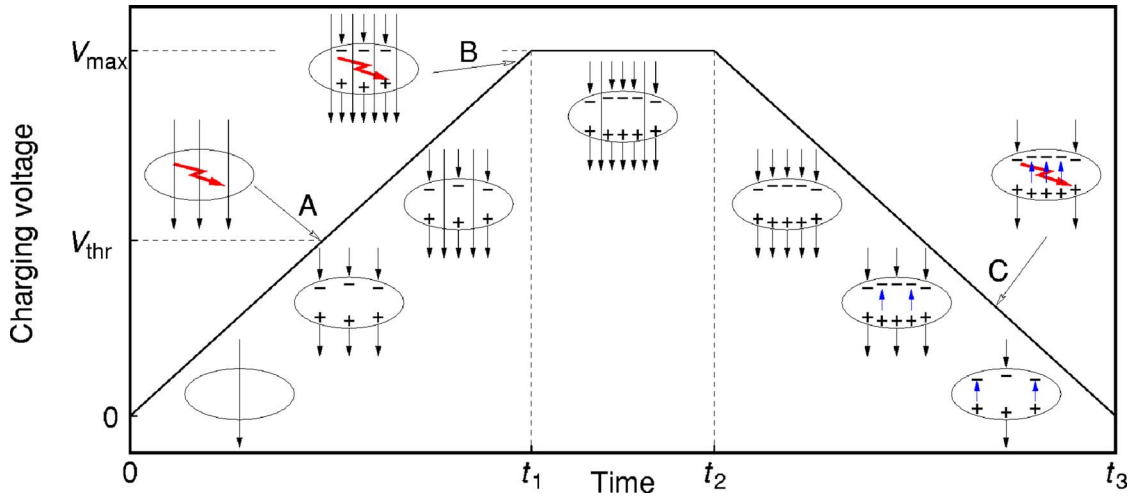


FIG. 2. (Color online) Schematic view of the electric field and trapped space charge in a single polymer void as a function of the applied voltage, which is ramped up from 0 to $V_{max}$, then kept constant for a period of time before being ramped down. Upon reaching the threshold voltage $V_{thr}$, Paschen breakdown is initiated (a). At high voltages, a second discharge may occur (b). During the ramp-down phase, the trapped charges build up a reverse electric field, leading to a back discharge (c).

$$\Phi_{\text{down}} = \int_{t_2}^{t_3} L(t)dt \tag{5}$$

(where $t_2$ and $t_3$ are again defined in Fig. 2) follows a similar curve, but is significantly weaker, reaching approximately 40% of $\Phi_{\text{up}}$.

The piezoelectricity of ferroelectrets is determined by the effective charge density $\sigma_{\text{eff}}$, the respective thicknesses of the air gaps $s_2$ and solid layers $s_1$ and Young's modulus $Y$ (cf. Sec. IV B). One should keep in mind that all samples in this study were prepared with the same parameters, so that $Y$ and $s_2$ show only slight sample-to-sample variations of 6% and 1%, respectively. $s_1$ can be considered a constant, since the bulk polymer is nearly incompressible compared to the voids. Therefore, the dependence of $d_{33}$ on the charging voltage is dominated by $\sigma_{\text{eff}}$, which in turn must then be correlated with the light emission $\Phi$. In particular, according to the model depicted in Fig. 2, the back discharge is expected to decrease $\sigma_{\text{eff}}$ from a possibly high value at $V_{\text{max}}$ to a smaller value in the absence of an external electric field. Verifying this hypothesis required measuring $d_{33}$ under an applied bias voltage, as described in Sec. IV B.

Additional insight into the charging process of ferroelectrets can be gained from spatially-resolved light-emission maps. Figure 4 shows photographs taken by an EMCCD camera for a maximum charging voltage of $V_{\text{max}}=6$ kV and a ramp rate of 6 kV/s. The onset of the light emission is at $t=0.5$ s (corresponding to $V=3$ kV), which again demonstrates the threshold behavior. Some of the larger voids near the surface facing the camera can be seen to discharge and back-discharge in a specific voltage range. To our knowledge, this represents the first time-resolved imaging of the discharge process in individual voids. Discharges from voids in the bulk of the sample are recorded as well, but, due to strong light scattering in cellular PP, are seen as a diffuse glow, rather than individually resolved point discharges.

By integrating the flux in a 9 mm diameter circle, the time-dependence of the total light emission can be obtained. Figure 5 shows that—as for the PMT data—there is one "charging" and one "back discharge" peak, although their intensity ratio is different in comparison to Fig. 1. Unlike the measurements in Fig. 1, where a fresh sample was used for each "ramp-up–hold–ramp-down" cycle, the samples investigated with the EMCCD camera underwent multiple cycles in order to improve the signal-to-noise ratio. Thus, when the voltage was ramped up from 0 to 6 kV, many voids already carried a charge, and therefore an internal electric field opposite to the applied field. These voids would, if at all, experience a discharge only at much higher charging voltages. Therefore, the intensity of the "charging" peak is reduced, while the "back discharge" peak remains largely unaffected by the history of the sample.

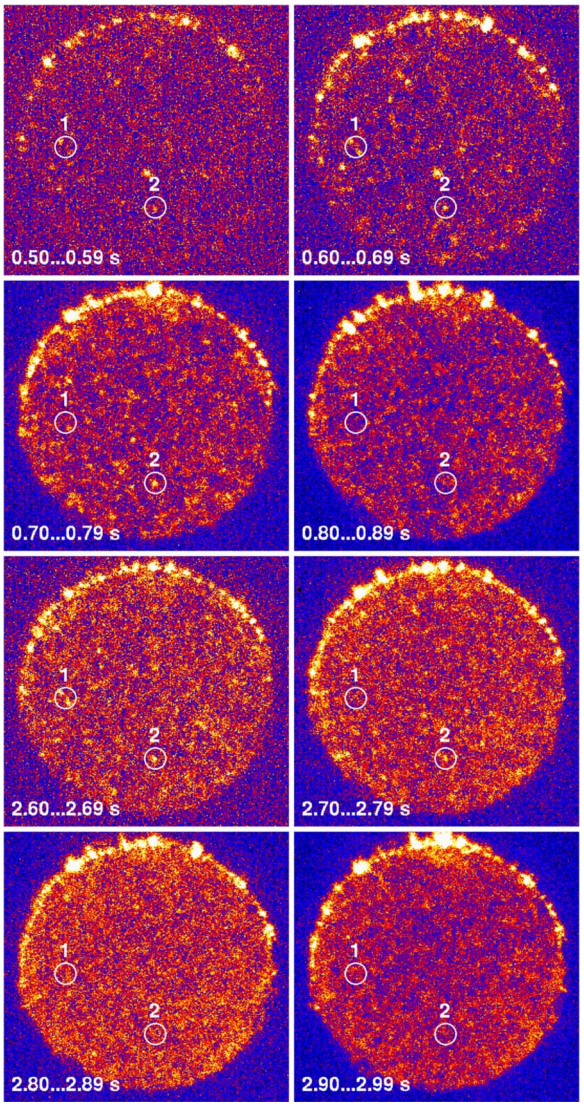


FIG. 4. (Color online) False-color EMCCD images of a cellular PP sample. The applied charging voltage was ramped up at a rate of 6 kV/s, starting at $t=0$, kept constant for 1 s and finally ramped down at a rate of −6 kV/s (cf. Fig. 5). Each frame was exposed for 90 ms. The images represent an average over 25 cycles. Circles 1 and 2 indicate light emission from some of the larger voids. The strong emission at the upper rim results from corona discharge at the electrode edge.

## B. Acoustic investigation of the actuator sensitivity and charge density

The discovery of the back discharge and the observed correlation between light emission and piezoelectric activity prompted the investigation of the piezoelectric $d_{33}$ coefficient during the charging process. An acoustic technique, using the inverse piezoelectric effect, was chosen due to its simplicity and its capability of measuring $d_{33}$ under an applied bias voltage. The acoustic signal as a function of the external bias voltage $V_{\text{bias}}$ is depicted in Fig. 6. When the maximum voltage of the cycle is lower than 3 kV, no difference in the sound signal is observed between ramping up and ramping down the external bias voltage. However, when the external bias voltage exceeds 3 kV, the sound signal during ramping up the external voltage is higher than the corresponding value during ramping down, and the difference grows with increasing maximum voltage of the cycle. As the voltage is reduced from its maximum value, $d_{33}$ reaches a minimum, then increases again as $V_{\text{bias}}$ passes through zero, forming a characteristic "butterfly" curve.

To understand the origin of this curve, we look at the change in thickness under an external voltage. According to a simplified model of ferroelectrets, $\Delta s$ can be expressed as[8]

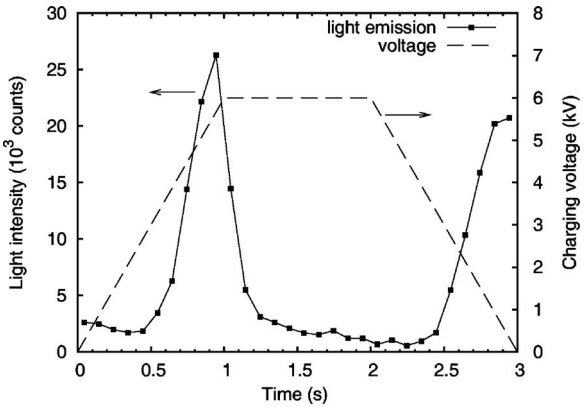


FIG. 5. Light intensity and charging voltage as a function of time. The light intensity was obtained from EMCCD images (cf. Fig. 4) by subtracting dark frames and integrating the flux in a circle of approximately 9 mm diameter, centered on the sample.

$$\Delta s = \frac{s}{Y}\frac{\varepsilon_p s_1 \sigma_{\text{eff}} V - \frac{1}{2}\varepsilon_0 \varepsilon_p^2 V^2}{(s_1 + \varepsilon_p s_2)^2}, \tag{6}$$

where $V$ is the external voltage applied to the electrodes, $Y$ is Young's modulus of the sample, $\varepsilon_0$ and $\varepsilon_p$ are the permittivity of vacuum and the relative permittivity of PP, respectively. $s_1$ and $s_2$ are the total thickness of the solid material layers and the gaseous layers, respectively, with $s=s_1+s_2$ being the total film thickness. $\sigma_{\text{eff}}=\Sigma s_{2i}\sigma_i/\Sigma s_{2i}$ is the effective charge density on the PP/air interfaces on both sides of the single air gap, where $s_{2i}$ is the thickness of the $i$th gaseous layer with $\Sigma s_{2i}=s_2$, and $\sigma_i$ is the charge density on the surface of the $i$th layer. In the numerator of Eq. (6), the first term is the piezoelectric contribution from the charged voids while the second term describes the Maxwell stress. The right-hand side of Eq. (6) has the opposite sign compared to that in Ref. 8 due to the fact that $\sigma_{\text{eff}}$ results from the very barrier discharge caused by the applied voltage $V$. Its polarity is such that the piezoelectric term in Eq. (6) makes the sample expand unless $V$ is reversed. The Maxwell stress term, on the other hand, always results in a compressive strain.

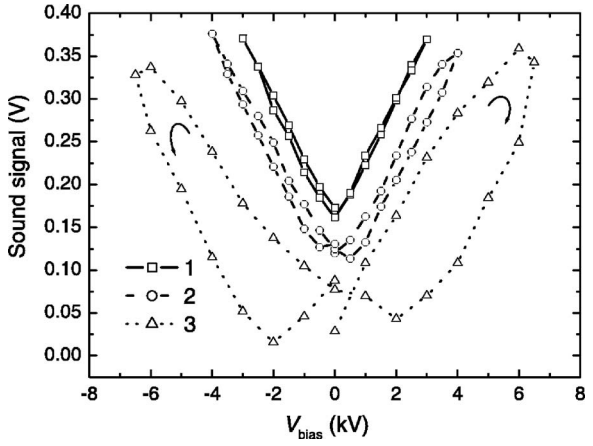


FIG. 6. Sound signal as a function of the external bias voltage applied to the electrodes. The positive half cycle is followed by the negative half cycle (the cycle direction is denoted by two arrows). The maximum voltages for each cycle are: (1) 3 kV, (2) 4 kV, and (3) 6 kV. Measurements were done on the same, previously uncharged sample from cycle 1 to 3. For clarity, the results of cycle (1) and (2) were shifted by 0.15 V and 0.1 V, respectively.

Applying a voltage $V=V_{\text{bias}}+V_0\sin(\omega t)$ where $V_0 \ll V_{\text{bias}}$, we obtain from Eq. (6)

$$\Delta s \approx \frac{s}{Y(s_1+\varepsilon_p s_2)^2}\left\{-\frac{1}{2}\varepsilon_0\varepsilon_p^2 V_{\text{bias}}^2 + \varepsilon_p s_1 \sigma_{\text{eff}} V_{\text{bias}} + \left[-\varepsilon_0\varepsilon_p^2 V_{\text{bias}} + \varepsilon_p s_1 \sigma_{\text{eff}}\right] V_0 \sin(\omega t)\right\}, \tag{7}$$

where the term proportional to $V_0^2$ has been neglected. Inspecting the last term in Eq. (7), we see that the radiated sound amplitude has a contribution not only from the effective charge density $\sigma_{\text{eff}}$, but also from the modulated Maxwell stress. The effective piezoelectric coefficient at $V_{\text{bias}}$ is then given by

$$d_{33} = \frac{s}{Y}\frac{\varepsilon_p s_1 \sigma_{\text{eff}} - \varepsilon_0 \varepsilon_p^2 V_{\text{bias}}}{(s_1+\varepsilon_p s_2)^2}. \tag{8}$$

The amplitude of the sound signal in Fig. 6 is proportional to the absolute value of $d_{33}$. In Ref. 8, an almost linear dependence of the piezoelectric sensitivity on the external voltage was observed within the range from −700 to +700 V. This is the expected behavior according to Eq. (8), since $\sigma_{\text{eff}}$ can be considered constant at an external voltage much lower than the threshold voltage. In the present work, however, a much higher external voltage was applied, and the actuator response of the sample was synchronously detected by an acoustic method. For cycles where the maximum $V_{\text{bias}}$ is lower than the threshold voltage, there is no hysteresis in the sound signal (Fig. 6) since the signal results from the reversible effect of the Maxwell stress only. Above a threshold voltage of approximately 3 kV, electric breakdown occurs in the voids, giving rise to an effective charge density $\sigma_{\text{eff}}$ which contributes to $d_{33}$ with the opposite sign of the Maxwell stress term in Eq. (8). As a result, the slope in Fig. 6 is reduced as $V_{\text{bias}}$ increases and a difference of the sound signal between ramping up and ramping down the external bias voltage appears.

The observed minimum in the sound signal vs. bias voltage occurs when the piezoelectric and Maxwell stress terms in Eq. (8) cancel each other. The small residual sound signal at this point can be attributed to a nonuniform spatial distribution of $\sigma_{\text{eff}}$. A phase shift of approximately 180° between the sound signal and the stimulating sinusoidal voltage is observed when the sound signal passes through its minimum in the "butterfly" curve due to the reversal of the polarity of the $d_{33}$ coefficient.

The acoustic measurements, only delivered relative (uncalibrated) $d_{33}$ values. In order to obtain absolute $d_{33}$ values, dielectric resonance spectroscopy was performed on the sample immediately after the external voltage cycles. Young's modulus and $d_{33}$ were determined by fitting the real part of the measured capacitance (inset of Fig. 7) to Eqs. (1)–(3). By comparing this $d_{33}$ value with the zero-field sound signal, all other sound signal measurements can be converted to piezoelectric $d_{33}$ coefficients.

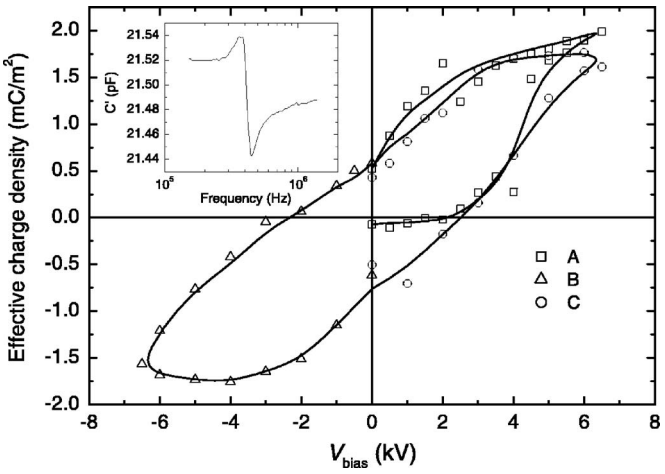


FIG. 7. Calculated effective charge density $\sigma_{\text{eff}}$ as a function of the bias voltage $V_{\text{bias}}$. A fresh, uncharged sample was used for the positive half cycle (a), followed by a negative half cycle (b), and subsequently a second positive half cycle (c). The inset shows a typical dielectric resonance spectrum from which the $d_{33}$ coefficient and $\sigma_{\text{eff}}$ were calculated.

Now that absolute $d_{33}$ values are available, $\sigma_{\text{eff}}$ can be calculated from $s_1$, $s_2$, $V_{\text{bias}}$, and $Y$ according to Eq. (8). This calculation assumes that $s_2$ and $Y$ remain constant. For $V_{\text{bias}}=6.5$ kV, the first (Maxwell stress) term in Eq. (7) is $-4.1$ $\mu$m. However, the actual bias thickness change is less than $-4.1$ $\mu$m because it is partly compensated by the second (piezoelectric) term. $Y$ can be considered as a constant within such a small thickness change. The quantities $s_1$ and $s_2$ were determined from the density of the samples given by the manufacturer and from the measured thickness, because the density of PP is known and the density of air is approximated as zero. The development of $\sigma_{\text{eff}}$ with $V_{\text{bias}}$ is clearly visible in Fig. 7, which shows a hysteresis behavior similar to that of traditional ferroelectrics. For a fresh, uncharged sample, $\sigma_{\text{eff}}$ is nearly zero when the external voltage is below 3 kV. The small negative effective charge density at $V_{\text{bias}}=0$ (corresponding to $d_{33}\approx 2$ pC/N) is due to charges deposited during the manufacturing process. Above the threshold voltage, $\sigma_{\text{eff}}$ increases to a maximum value of 2.0 mC/m$^2$. However, a significant reduction of $\sigma_{\text{eff}}$ is observed when the external voltage decreases from its maximum to a value below 3 kV, which again proves the back barrier discharge. A zero-field $\sigma_{\text{eff}}$ value of about 0.5 mC/m$^2$ is obtained, analogous to the remanent polarization in ferroelectrics. This value is in very good agreement with values determined by Sessler *et al.*[6] and Paajanen *et al.*[8] on other types of cellular PP ferroelectrets. Somewhat more accurate values could be expected if the thickness change was directly measured by, e.g., an interferometric method.

## V. CONCLUSION

Light emission from barrier discharges in the voids of ferroelectrets shows the same threshold behavior as the piezoelectricity of the respective material. For pressure-inflated PQ50 ferroelectrets, the emission starts above a threshold voltage of 3 kV and then significantly increases with the applied voltage. In addition, a second "back discharge" emission is observed when the voltage is reduced toward zero. The discharge events in individual voids are revealed by time-resolved images.

Direct contact charging of pressure-inflated PQ50 ferroelectrets with varying voltage leads to a polarization-voltage ($P$-$V$) hysteresis curve, from which a threshold charging voltage of 3 kV and the back barrier discharges were confirmed and a zero-field "effective polarization" of 0.5 mC/m$^2$ was determined. Our results suggest that the piezoelectricity of ferroelectrets would be significantly improved if the back discharge could be suppressed, since it destroys a significant fraction of the effective charge density.

## ACKNOWLEDGMENTS

We thank Dr. Guggi Kofod and Dr. Steffen Bergweiler (both University of Potsdam) for many stimulating discussions. We are also indebted to Professor Martin Ostermeyer and Markus Gregor from the Nonlinear Optics group at the University of Potsdam for providing the EMCCD camera.

[1] S. Bauer, R. Gerhard-Multhaupt, and G. M. Sessler, Phys. Today **57**, 37 (2004).
[2] M. Wegener and S. Bauer, ChemPhysChem **6**, 1014 (2005).
[3] M. Wegener, Mater. Sci. Eng., R.: Reports (in press).
[4] M. Lindner, H. Hoislbauer, R. Schwödiauer, S. Bauer-Gogonea, and S. Bauer, IEEE Trans. Dielectr. Electr. Insul. **11**, 255 (2004).
[5] G. M. Sessler and J. Hillenbrand, Appl. Phys. Lett. **75**, 3405 (1999).
[6] J. Hillenbrand, G. M. Sessler, and X. Zhang, J. Appl. Phys. **98**, 064105 (2005).
[7] M. Paajanen, H. Välimäki, and J. Lekkala, *Proceedings of the 10th International Symposium on Electrets, Delphi, Greece, 22–24 September, 1999* (IEEE Service Center, Piscataway, NJ, 1999), pp. 735–738.
[8] M. Paajanen, J. Lekkala, and H. Välimäki, IEEE Trans. Dielectr. Electr. Insul. **8**, 629 (2001).
[9] E. Tuncer, J. Phys. D **38**, 497 (2005).
[10] M. Wegener, W. Wirges, and R. Gerhard-Multhaupt, Adv. Eng. Mater. **7**, 1128 (2005).
[11] W. Wirges, M. Wegener, O. Voronina, L. Zirkel, and R. Gerhard-Multhaupt, Adv. Funct. Mater. **17**, 324 (2007).
[12] E. Saarimäki, M. Paajanen, A. Savijärvi, M. Wegener, O. Voronina, R. Schulze, W. Wirges, and R. Gerhard-Multhaupt, IEEE Trans. Dielectr. Electr. Insul. **13**, 963 (2006).
[13] I. Graz, M. Kaltenbrunner, C. Keplinger, R. Schwödiauer, S. Bauer, S P. Lacour, and S Wagner, Appl. Phys. Lett. **89**, 073501 (2006).
[14] J. Hillenbrand and G. M. Sessler, J. Acoust. Soc. Am. **116**, 3267 (2004).
[15] X. Zhang, J. Hillenbrand, and G. M. Sessler, J. Phys. D **37**, 2146 (2004).
[16] M. Wegener, W. Wirges, J. Fohlmeister, B. Tiersch, and R. Gerhard-Multhaupt, J. Phys. D **37**, 623 (2004).
[17] M. Wegener, W. Wirges, R. Gerhard-Multhaupt, M. Dansachmüller, R. Schwödiauer, S. Bauer-Gogonea, S. Bauer, M. Paajanen, H. Minkkinen, and J. Raukola, Appl. Phys. Lett. **84**, 392 (2004).
[18] M. Paajanen, M. Wegener, and R. Gerhard-Multhaupt, J. Phys. D **34**, 2482 (2001).
[19] X. Qiu, M. Wegener, W. Wirges, X. Zhang, J. Hillenbrand, Z. Xia, R. Gerhard-Multhaupt, and G. M. Sessler, J. Phys. D **38**, 649 (2005).
[20] M. Lindner, S. Bauer-Gogonea, S. Bauer, M. Paajanen, and J. Raukola, J. Appl. Phys. **91**, 5283 (2002).
[21] U. Kogelschatz and J. Salge, in *Low Temperature Plasma Physics, Fundamental Aspects and Applications*, edited by R. Hippler, S. Pfau, M. Schmidt, and K. H. Schoenbach (Wiley VCH, New York, 2001), Chap. 13, pp. 331–357.
[22] U. Kogelschatz, Pure Appl. Chem. **62**, 1667 (1990).
[23] G. Oversluizen, M. Klein, S. De Zwart, S. Van Heusden, and T. Dekker, Appl. Phys. Lett. **77**, 948 (2000).
[24] U. Kogelschatz, Plasma Chem. Plasma Process. **23**, 1 (2003), and references therein.

[25]M. Wegener, M. Paajanen, W. Wirges, and R. Gerhard-Multhaupt, *Proceedings of the 11th International Symposium on Electrets, Melbourne, Australia, 1–3 October, 2002* (IEEE Service Center, Piscataway, NJ, 2002), pp. 54–57.
[26]S. Zhukov and H. von Seggern, J. Appl. Phys. **101**, 084106 (2007).
[27]A. Savolainen and K. Kirjavainen, J. Macromol. Sci., Chem. **A26**, 583 (1989).
[28]A. Mellinger, IEEE Trans. Dielectr. Electr. Insul. **10**, 842 (2003).
[29]H. Ohigashi, J. Appl. Phys. **47**, 949 (1976).
[30]G. S. Neugschwandtner, R. Schwödiauer, M. Vieytes, S. Bauer-Gogonea, S. Bauer, J. Hillenbrand, R. Kressmann, G. M. Sessler, M. Paajanen, and J. Lekkala, Appl. Phys. Lett. **77**, 3827 (2000).